An Electrostatic MEMS Actuator with Large Displacement Under Low Driving Voltage*

Ming Anjie[1,2,†], Li Tie[1], Zhou Ping[1], and Wang Yuelin[1]

(1 *State Key Laboratory of Transducer Technology, National Key Laboratory of Microsystem Technology, Shanghai Institute of Microsystem and Information Technology, Chinese Academy of Sciences, Shanghai* 200050, *China*)
(2 *Graduate University of the Chinese Academy of Sciences, Beijing* 100049, *China*)

Abstract: A comb-drive actuator for lateral movement of over 100μm under low driving voltage is designed. Side stability is analyzed to improve the performance of the actuator. According to the analysis, a comb-drive actuator with small comb gap, high-stiffness-ratio prebent suspension beams, non-initial overlap, and linear-engaged-length comb teeth is proposed and the parameters of the actuator are derived. Experiments indicate that the actuator resonates at 573Hz with a Q factor of 35.88 and reaches a maximum displacement of over 100μm at a driving voltage of 71V, which fulfills the design requirements and matches the analytical value to within 2.1%.

Key words: comb-drive actuator; side stability; MEMS
EEACC: 2575
CLC number: TM402 **Document code**: A **Article ID**: 0253-4177(2008)09-1703-05

1 Introduction

Electrostatic actuation is very popular among MEMS actuators and lateral electrostatic comb-drive actuators are useful because of their linear electrical transfer function, large displacement, and high quality factor in contrast to parallel-plate capacitive drivers. More than 15 years ago, Tang *et al*.[1] introduced a comb-drive actuator to the MEMS field. However, the stable travel range or the maximum stable displacement of the conventional comb-drive actuator is limited by the electromechanical side instability, namely, the side pulling effect[2,3]. Grade *et al*.[4] improved a comb drive actuator that provided a displacement of up to 100μm, but its driving voltage is higher than 150V, which is unsuitable for some applications.

In this paper, a smart design is presented, simulated, and fabricated with a small comb gap, two banks of comb teeth, and two pairs of slim prebent suspension beams to achieve large deflection under a low driving voltage. Experimental results indicate that the actuator can achieve 100μm movement under 71V.

2 Analysis

2.1 Side stability analysis

A typical comb-drive actuator put forward by Tang *et al*.[1] is symmetric about both the x- and y-axes and has four folded-beam suspension springs. An engaged pair of teeth of a comb actuator is shown schematically in Fig. 1.

When a driving voltage, V, is applied between the movable and the fixed teeth, the electrostatic force in the lateral direction is given by

$$F_x = \frac{1}{2} \times \frac{\mathrm{d}C}{\mathrm{d}x} V^2 = \frac{N\varepsilon h \omega_c V^2}{(l_c - x)^2} + \frac{N\varepsilon h V^2}{2}\left(\frac{1}{g - \delta_y} + \frac{1}{g + \delta_y}\right) \quad (1)$$

Besides electrostatic force along the x-direction, there is also electrostatic force along the y-axis:

$$F_{ey} = \frac{1}{2} \times \frac{\mathrm{d}C}{\mathrm{d}y} V^2 = \frac{N\varepsilon h (L_0 + \delta_x) V^2}{2(g - \delta_y)^2} - \frac{N\varepsilon h (L_0 + \delta_x) V^2}{2(g + \delta_y)^2} \quad (2)$$

where N is the number of comb teeth, ε is the dielectric constant of air, h is the comb teeth height, x is

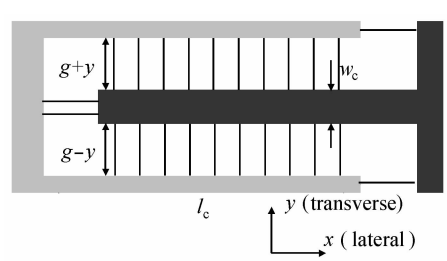

Fig. 1 Schematic drawing of a single comb pair illustrating the parallel-plate model

* Project supported by the State Key Development Program for Basic Research of China (No. 2006CB30040)
† Corresponding author. Email: maj6666@163.com
Received 30 November 2007, revised manuscript received 26 March 2008

the distance the combs are engaged, δ_y is a small displacement departure along the y-direction, δ_x is the comb displacement in the x-direction, g is the comb gap between the teeth, and ω_c and l_c are the width and length of a comb tooth, respectively.

Here, following Grade *et al*.[4], we define the stability parameter, S, as the ratio of the sideways suspension restoration forces to the sideways electrostatic forces. S can be represented as

$$S = \frac{k_y g^2}{2k_x \delta_x^2} = \frac{4g^2 L_b^2}{\delta_x^2 (3\delta_x^2 + 8b^2)} \tag{3}$$

where $k_x = Ehb^3/L_b^3$, $k_y = Ehb/L_b$, are the spring constants of the suspension beam in the forward direction and transverse direction, and L_b and b are the length and width of the suspension beam.

The magnitude of S represents the degree of side stability of the actuator. For stability, the parameter S must be slightly larger than one throughout the full movement in the x-direction[5,6].

2.2 Tolerance effects on side stability

For a fabricated actuator, non-ideal mechanical behavior, dimension offset, and non-ideal mechanical behavior will affect the side stability. Therefore, it is necessary to analyze their effects to produce the necessary side stability.

The dimensional offset, e, is defined as the increase in the width of the comb teeth and the suspension beams. As the comb gap and beam width varies, the side electrostatic force and the spring constants k_x, k_y will be modified. Thus, the side stability can be expressed by

$$S_e = \frac{L_b^2 (g - e)^2}{2\delta_x^2 (b + e)^2} \tag{4}$$

In this case, the stable equilibrium is also considered, i.e., $\delta_y = 0$. Thus, the stability ratio due to the dimensional offset can be described as

$$\frac{S_e}{S} = \frac{(g - e)^2}{g^2} \times \frac{b^2}{(b + e)^2} \tag{5}$$

The ratio as a function of the offset is shown in Fig. 2 for an actuator with 8μm wide suspension-beams, a 7μm wide comb teeth, and 2μm wide comb gaps. When the dimension error is 0.25μm, the side-stability will decrease by 26%.

In practice, the sidewalls may slope inward or outward after a deep reactive ion etch (DRIE) process. The etched slanted trench is schematically shown in the inset of Fig. 2. These fabrication tolerances, especially the etched profile gauged by the angle θ (counterclockwise from the reference vertical line to the sidewall), affect the performances of the fabricated actuator in terms of side stability, as discussed in Refs. [6~8]. But in those works, only the

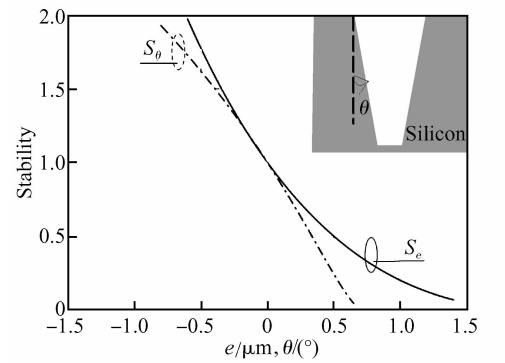

Fig. 2 Stability ratio versus dimensional offset and sidewall sloped angle of both comb teeth and folded-beam suspension

imperfect vertical profile of the folded suspension beam is considered. In fact, the sidewall angular errors of the comb teeth and the suspension beams greatly affect the stability also.

According to the definition of side stability and Eq. (2), the side stability considering a slanted sidewall can be derived as

$$S_\theta = \frac{k_y g^2}{2k_x \delta_x^2} \times \frac{2(90g - \pi h\theta)^2 \ln\zeta}{\pi h\theta (180g - \pi h\theta)} \tag{6}$$

where ζ represents $g/(g - \pi h\theta/90)$. As the real angle θ is very small, $\tan\theta$ is approximated to θ during the derivation of Eq. (6). Comparing Eq. (6) for side stability with the initial stability, we also have the ratio

$$\frac{S_\theta}{S} = \frac{2(90g - \pi h\theta)^2 \ln z}{\pi h\theta (180g - \pi h\theta)} \tag{7}$$

This stability ratio as a function of the sloped angle under the same condition can be found in Fig. 2. When the sloped angle is positive 0.3°, the side stability is reduced by 45%.

Non-ideal mechanical behavior causes the actuator to follow a trajectory that contains a small sideways component without side electrostatic forces[7]. The stability of the comb actuator will decrease by 29% for this comb misalignment.

In our case, the employed process can only be expected in a dimension of ±0.25μm and a sidewall angle of ±0.3°. In other words, the worst dimensional offset and slanted sidewall will result in a decrement of 26% and 45% to the side stability, respectively. With the 29% reduction of stability from non-ideal mechanical behavior, the initial stability should be larger than 3.5 to keep it work properly.

2.3 Approach to improve side stability and decrease driving voltage

Equation (2) indicates that the net electrostatic force in the y direction F_{ey} will push the movable teeth further off the equilibrium if it leaves the original equilibrium position. It looks like there is a 'negative' spring.

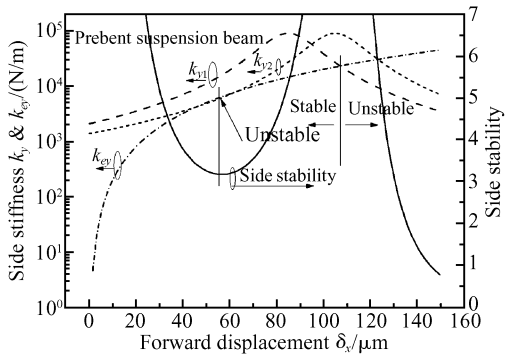

Fig. 3　Analytical results of the spring constants k_{y1} (x_{pb} = 50μm), k_{y2} (x_{pb} = 60μm), and k_{ey} (short dashed-dotted line) as functions of the displacement δ_x, and the side stability (solid line) versus forward deflection

The equivalent 'negative' spring constant k_{ey} is defined as[10]

$$k_{ey} = \left.\frac{\partial F_{ey}}{\partial y}\right|_{y=\delta y} = N\varepsilon hV^2(L_0 + \delta_x)\left(\frac{1}{(g-\delta_y)^3} + \frac{1}{(g+\delta_y)^3}\right) \quad (8)$$

The maximum stable displacement δ_x can be expressed by

$$\delta_x^{\max} = -\frac{L_0}{2} + \frac{1}{2}\sqrt{L_0^2 + 2\frac{k_y}{k_x}g^2} \quad (9)$$

According to Eqs. (1), (4), and (9), the larger the comb gap, the higher the side stability, but the needed driving voltage is also higher. Therefore, an effective way to improve side stability is to properly design the suspension beams and comb finger profile.

It is in fact the upper limits of the spring constant in the y-direction at small lateral deflection for $k_y = Ehb/L_b$[5,11]. Finally, the side spring constant in the y-direction is given by

$$k_y = \frac{8Ehb^3}{3L_b\delta_x^2 + 8L_b b^2} \quad (10)$$

The side stability or the stable forward deflection may be dramatically increased if the suspension beams straighten at a forward deflection x_{pb}. Figure 3 shows that the two beams' maximum spring stiffness k_y shift from zero to 85 and 105μm, respectively. The side stability of the prebent suspension beam indicates that it is low initially and increases as the suspension beams straighten with forward deflection and the side stability is dramatically increased for relatively large deflection. The spring constant k_y at small δ_x decreases with the increment of the parameter x_{pb}. Therefore, x_{pb} cannot be too large for certain suspension beams.

Figure 4 shows a schematic diagram of one prebent suspension beam. The beam profile (solid line), $w(y)$, can be found using the following differential equation[12]:

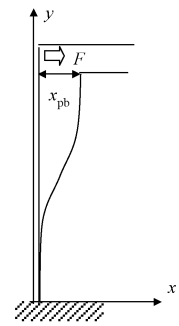

Fig. 4　Schematic drawing of a fixed-guided beam with length l (The solid outline is the beam displaced by x_{pb}.)

$$-EIw''(y) = -F(l-y) \quad (11)$$

The boundary conditions for the fixed-guided beam are $w(0) = 0$, $w'(0) = 0$, $w(l) = 0$, and $w'(l) = 0$. Then the solution to Eq. (12) can be found.

$$w(y) = c\left(\frac{ly^2}{2} - \frac{y^3}{3}\right) \quad (12)$$

where c represents $F/2EI$ and $I = bh^3/12$ is the moment of inertia of the beam. The maximum displacement, w_{max}, at the free end (i.e., at $y = l$) is

$$w_{max}(y) = x_{pb} = cl^3/6 \quad (13)$$

According to Eqs. (12) and (13), the deflected beam profile can be determined.

Another way to improve side stability is to reduce the overlap area[2]. There are two ways to achieve this: reducing the initial overlap length of the comb teeth or adjusting the lengths of the individual comb teeth. Here, a non-initial overlapping comb-drive actuator with linear engagement comb teeth is adopted. Figure 5 demonstrates that the linear engagement comb-drive actuator has a maximum electrostatic force as large as equal to the length of the comb teeth and does not increase driving voltage to achieve the same maximum.

3　Design and simulation

The basic parameters in the comb-drive design

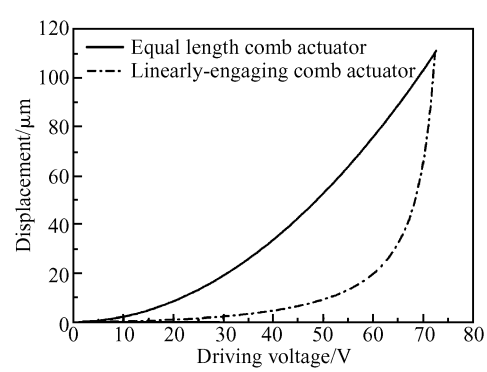

Fig. 5　Plot of predicted static deflection versus the driving voltage for actuators with equal-length combs and linearly-engaging combs

Table 1 Structural dimensions

Structure		Comb teeth	Suspension beam	Comb gap
Length /μm	Max	104	1200	1.5
	Min	30		
Width/μm		8	7	
Height/μm		90	90	
Total number (pair)		98	2	

are the dimensions of the suspension beams, the dimensions of the comb teeth, the number of comb teeth, the comb engagement profile, and x_{pb}.

The width of the suspension beam and comb teeth are limited by the fabrication process and are usually set to the minimum in order to achieve the minimum device area. The folded beam length, L, is used as the free parameter during the definition of comb gap. According to Eq. (10), replacing δ_x with $(\delta_x - x_{pb})$ and solving for g gives:

$$g = \frac{\delta_x}{L_b}\sqrt{2S\left(\frac{3}{8}(\delta_x - x_{pb})^2 + b^2\right)} \tag{14}$$

According to Eq. (1) and Hooker's law, the driving voltage of a linearly engaged comb-drive actuator can be derived as

$$V = \sqrt{\frac{2F_{max}g}{(2N-1)h\varepsilon}} = \sqrt{\frac{2Eb^3 g\delta_x}{(2N-1)L_b^3\varepsilon}} \tag{15}$$

The parameters of comb-drive are determined in Table 1.

The frequencies of the resonant modes may be modeled using the commercial software CoventorWare. The frequency of the first resonate mode is 638Hz. The second mode with a frequency of 2.62kHz occurs at about four times the first resonant frequency and the frequency separation is large enough to prevent excitation of the second mode, which is not desirable.

4 Results and discussion

The fabrication sequences are as follows. The fabrication starts with a 500μm thick Pyrex 7740 glass. Then, TiW/Au metal layers of 30nm/300nm are sputtered and opened through KI + I_2 etching. Next, the glass substrate is etched in 40% HF solution to form the cavity. Then, a 500μm thick (100) p-type 100mm silicon wafer is ground and polished to 100μm. DRIE (STS) is used to form the structure with a depth of 80μm followed by anodic silicon-glass bonding. Finally, the structures are released during the final DRIE process. The fabricated comb-drive actuator is shown in Fig. 6. The measured comb gap is about 2μm.

Capacitance measurement is used to quantify the

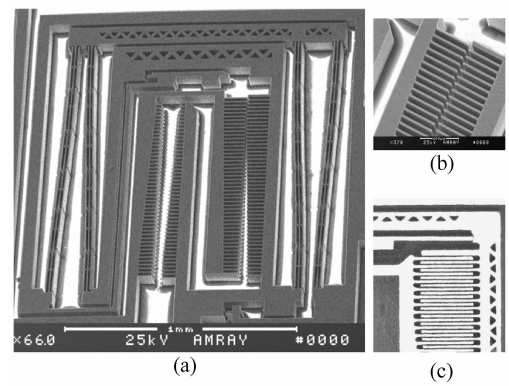

Fig. 6 (a) Microscope photo of the comb-drive actuator; (b) Close-up view of non-initial overlap comb teeth; (c) Close-up view of comb teeth and mechanical stop when voltage is applied

resonant behavior of the actuators and the first resonant frequency and Q factor are measured. The comb-drive actuator is bonded on a JZK vibrator with comb teeth in parallel with the vibrate direction. The vibrator connects with an XD7 voltage source, whose amplitude and frequency are tunable. The capacitance, which is proportional to the overlapping length of the comb teeth, is measured and then converted to voltage signals by a capacitance/voltage converting circuit before analysis by an HP4395 network analyzer. Figure 7 indicates that the measured first resonant frequency of the fabricated comb-drive actuator with suspension length of 1200μm and width of 7μm is 573Hz and the quality factor is 35.88. The measured resonant frequency agrees to within 10% of the simulation in Coventorware owing to slide-film air damping between moving comb structures and glass substrate and the changes in suspension width caused by fabrication errors.

Figure 8 shows the forward deflection as a function of the voltage squared for the comb-drive actuator. When the driving voltage reaches 71V, the actuator reaches a displacement of 100μm. The result matches the predicted driving voltage to within 2.1%.

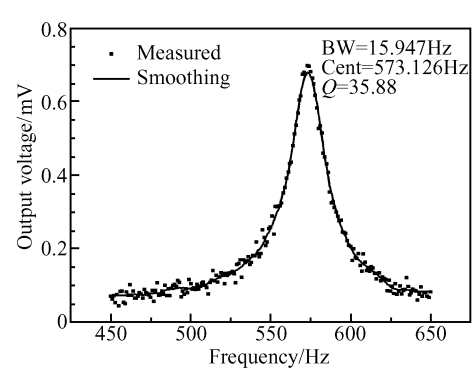

Fig. 7 Plot of measured output voltage versus vibration frequency of vibrator

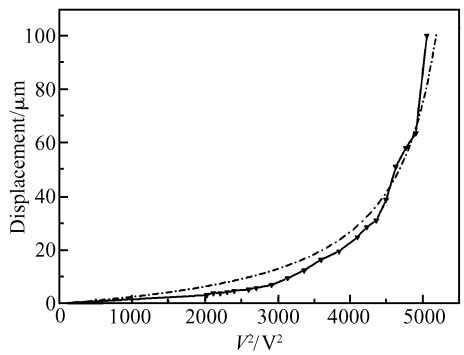

Fig.8　Plot of voltage squared versus the measured (solid line with symbol) and predicted (dashed line) static deflection

5　Conclusion

In this paper, side stability is analyzed first. Then, a smart comb-drive actuator is proposed and the parameters of the actuator are derived. Finally, experimental results indicate that the first resonant frequency is about 573Hz, which agrees to within 10% of the simulation, and the quality factor is approximately 35. The measured driving voltage is 71V, which fulfills the design requirement and matches the analytical value to within 2.1%. This actuator can be used on tunable applications in integrated actuators, sensors, and signal processing chips.

References

[1] Tang W C, Nguyen T H, Howe R T. Laterally driven polysilicon resonant microstructures. Sensors and Actuators A, 1989, 20: 25

[2] Brenner R A, Pisano A P, Tang W C. Multiple mode micromechanical resonators. Proc IEEE Micro Electro Mech Syst, Napa Valley, CA, 1990: 9

[3] Judy M W, Howe R T. Polysilicon hollow beam lateral resonators. Proc IEEE Micro Electro Mech Syst, Fort Lauderdale, FL, 1993: 265

[4] Grade J D, Jerman H, Kenny T W. A large-deflection electrostatic actuator for optical switching applications. Technical Digest of Solid State Sensor and Actuator Workshop, Hilton Head, SC, 2000: 97

[5] Huang Wei, Lu Ganyu. Analysis of lateral instability of in-plane comb drive MEMS actuators based on a two-dimensional model. Sensors and Actuators A, 2004, 113: 78

[6] Zhou G, Dowd P. Tilted folded-beam suspension for extending the stable travel range of comb-drive actuators. J Micromech Microeng, 2003, 13: 178

[7] Grade J D, Jerman H, Kenny T W. Design of large deflection electrostatic actuators. J Microelectromech Syst, 2003, 12: 335

[8] Li J, Liu A Q, Zhang Q X. Tolerance analysis for comb-drive actuator using DRIE fabrication. Sensors and Actuators A, 2006, 125: 494

[9] Chen Chihchung, Lee Chengkuo. Design and modeling for comb drive actuator with enlarged static displacement. Sensors and Actuators A, 2004, 15: 530

[10] Legtenberg R, Groeneveld A W, Elwenspoek M. Comb-drive actuators for large displacements. J Micromech Microeng, 1996, 6: 320

[11] Bochobza-Degani O, Elata D, Nemirovsky Y. A general relation between the ranges of stability of electrostatic actuators under charge or voltage control. Appl Phys Lett, 2003, 82: 302

[12] Bao Minghang. Analysis and design principles of MEMS devices. Elsevier, 2005

大位移低电压的静电 MEMS 驱动器*

明安杰[1,2,†]　李　铁[1]　周　萍[1]　王跃林[1]

(1 中国科学院上海微系统与信息技术研究所 传感技术联合国家重点实验室，微系统技术国家级重点实验室，上海　200050)
(2 中国科学院研究生院，北京　100049)

摘要： 制作了一种低驱动电压、位移达 100μm 的梳齿驱动器. 为了增加驱动器的驱动位移，对驱动器的侧向稳定性进行了分析. 根据分析结论，提出了一种采用小梳齿间隙，高纵/横向弹性常数比预弯曲支撑梁，无初始交叠、梳齿长度线性递增的梳齿驱动器. 根据稳定性以及驱动位移和驱动电压的设计要求设计了驱动器的具体参数，并进行了器件制作. 测试表明，器件共振点在 573Hz，Q 因子为 35.88，在 100μm 位移时驱动电压为 71V，与理论计算值相差 2.1%.

关键词： 梳齿驱动器；侧向稳定性；MEMS
EEACC： 2575
中图分类号： TM402　　**文献标识码：** A　　**文章编号：** 0253-4177(2008)09-1703-05

* 国家重点基础研究发展计划资助项目(批准号：2006CB30040)
† 通信作者. Email: maj6666@163.com
2007-11-30 收到，2008-03-26 定稿